The Cryosphere

Discussions

Open Access

EGU

Modelling the Antarctic Ice Sheet across the Mid Pleistocene Transition - Implications for Oldest Ice

Johannes Sutter[1,2], Hubertus Fischer[2], Klaus Grosfeld[1], Nanna B. Karlsson[1], Thomas Kleiner[1], Brice Van Liefferinge[3,5], and Olaf Eisen[1,4]

[1]Alfred Wegener Institute Helmholtz-Centre for Polar and Marine Research, 27568 Bremerhaven, Germany
[2]Climate and Environmental Physics, Physics Institute, and Oeschger Centre for Climate Change Research, University of Bern, Bern, Switzerland
[3]Laboratoire de Glaciologie, Université libre de Bruxelles, CP 160/03, Avenue F.D. Roosevelt 50, B-1050 Brussels, Belgium
[4]Department of Geosciences, University of Bremen, Bremen, Germany
[5]Norwegian Polar Institute Fram Centre, NO-9296, Tromsø, Norway

Correspondence: Johannes Sutter (johannes.sutter@awi.de)

Abstract. The international endeavour to retrieve a continuous ice core, which spans the middle Pleistocene climate transition ca. 1.2-0.9 Myr ago, encompasses a multitude of field and model-based pre-site surveys. We expand on the current efforts to locate a suitable drilling site for the oldest Antarctic ice core by means of 3D continental ice sheet modelling. To this end, we present an ensemble of ice sheet simulations spanning the last 2 Myr and employing transient boundary conditions

5 derived from climate modelling and climate proxy records. We discuss the effects of changing climate conditions, sea level and geothermal heat flux boundary conditions on the mass balance and ice dynamics of the Antarctic Ice Sheet. Our modelling results show a range of configurational ice sheet changes across the middle Pleistocene transition, suggesting a potential shift of the West Antarctic Ice Sheet to a marine-based configuration. Despite the middle Pleistocene climate re-organisation and associated ice-dynamic changes we identify several regions conducive to conditions maintaining 1.5 Myr old ice, particularly

10 around Dome Fuji, Dome C and Ridge B, in agreement to previous studies. This finding strengthens the notion that old ice exists in previously identified regions, while providing a dynamic continental ice sheet context.

Copyright statement. TEXT

1 Introduction

The middle Pleistocene transition (MPT) is characterised by a shift from obliquity driven climate cycles (~ 41 ka) to the

15 signature sawtooth ~ 100 ka cycles typical for the late Pleistocene. The drivers behind the MPT are still under debate and touch on the basic understanding of the climate system. The absence of any clear disruptive change during the MPT in orbital forcing makes the transition especially puzzling. Several theories have been put forth, striving to explain the enigmatic MPT (Raymo and Huybers, 2008). They include a shift in subglacial conditions underneath the Laurentide Ice Sheet (regolith hypothesis by Clark and Pollard (1998)), the inception of a large North American Ice Sheet (Bintanja and van de Wal, 2008) or marine East

Antarctic Ice Sheet by Raymo et al. (2006), ice bedrock climate feedbacks (Abe-Ouchi et al., 2013), the buildup of large Ice Sheets between MIS24 and 22 identified by Elderfield et al. (2012), or the combination of changes of ice sheet dynamics and the carbon cycle (Chalk et al., 2017). Ultimately, it seems likely that an interplay of the various proposed processes culminated in the MPT. To illuminate the potential role of these different processes and thus to solve one of the grand challenges of climate

5 research, the recovery of a continuous ice core spanning at least the MPT (in the following termed as "Oldest Ice") is crucial. An expansion of the currently longest ice core record from the EPICA Dome C project (Jouzel et al., 2007) to and beyond the MPT, would provide the necessary atmospheric boundary conditions to revisit the current theories (Fischer et al., 2013). It would provide a direct record of global atmospheric CO_2 and CH_4 concentrations and local climate during the MPT and beyond. A transient record of CO_2 concentrations would provide a key piece of the puzzle in answering the question whether

10 greenhouse gases were the main culprit behind the MPT, while proxies of climate conditions in Antarctica would illuminate the evolution of the Antarctic Ice Sheet leading to the MPT. However, retrieval of such an ice core is a challenging task, as a multitude of prerequisites must be met (Fischer et al., 2013; Van Liefferinge and Pattyn, 2013; Parrenin et al., 2017) to recover an undisturbed ice core reaching more than a million years into the past. The IPICS-community (International Partnership in Ice Core Sciences) has identified the most promising targets for an Oldest Ice drill site close to a secondary dome in the

15 vicinity of Dome C, usually referred to as "Little Dome C" (LDC) (Parrenin et al., 2017) and other potential targets around Dome Fuji. The selection of sites is motivated by a series of recent studies based both on radar observations of the internal ice sheet stratigraphy and underlying bedrock topography (Young et al., 2017; Karlsson et al., 2018), local paleoclimate conditions (Cavitte et al., 2018), as well as 1D and 3D flow modelling (Van Liefferinge et al., 2018; Parrenin et al., 2017; Passalacqua et al., 2017). These studies provide a detailed view on the regional properties such as ice flow, thermal conditions and bedrock

20 topography, enabling a localized estimate of promising drill sites. The only component missing so far in the analysis is the transient, continental paleo ice sheet dynamics perspective, which allows for the assessment of large-scale re-organizations of ice sheet flow and geometry during glacial and interglacial cycles, their impact on divide migration, ice thickness changes along the East Antarctic ice divide and basal melt. There are many studies focussing on the dynamics of the AIS during specific climate episodes in the past such as the Last Interglacial (LIG) (Sutter et al., 2016; DeConto and Pollard, 2016) or the Last

25 Glacial Maximum (LGM) (e.g. Golledge et al., 2014). However, so far only a few studies cover the waxing and waning of the AIS during the MPT (Pollard and DeConto, 2009; de Boer et al., 2014) or late Quaternary (Tigchelaar et al., 2018) in transient model simulations with an evolving climate forcing. We build on these efforts by carrying out ensemble simulations of the Antarctic Ice Sheet across the last 2 Myr to investigate the MPT and the effect of ice sheet dynamics on potential Oldest Ice drill sites.

30 ## 2 Methods

2.1 Ice Sheet Model

We employ the 3D thermomechanical Parallel Ice Sheet Model (PISM) (Bueler and Brown, 2009; Winkelmann et al., 2011) in the hybrid shallow-shelf/shallow-ice mode (ssa+sia) with a subgrid grounding line parameterisation (Gladstone et al., 2010;
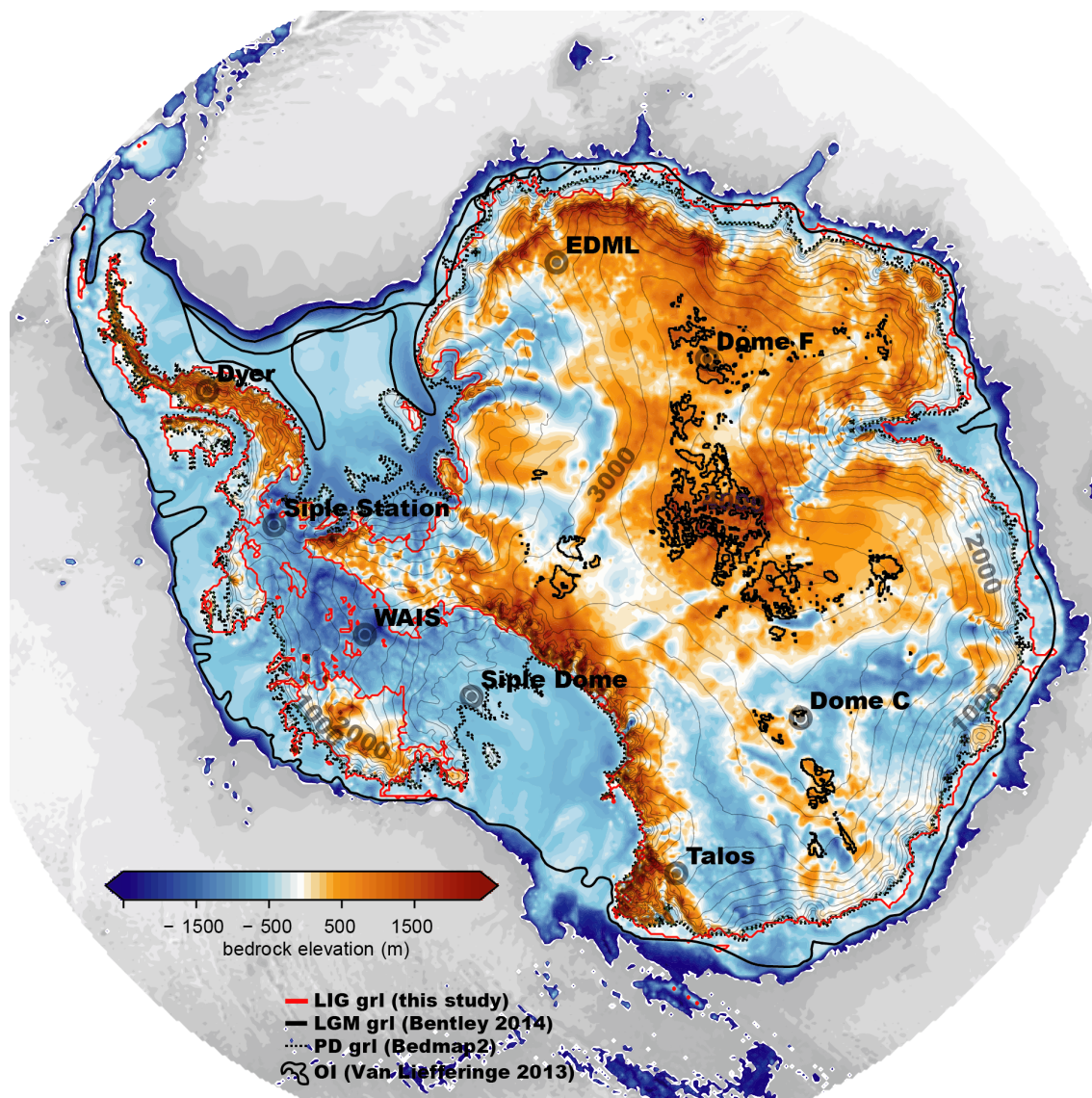
Figure 1. Antarctic bedrock topography overlain by surface contour (gray lines). The present day (PD) grounding line from BEDMAP2 (Fretwell et al., 2013) is depicted by the dashed black line, Last Glacial Maximum (LGM) grounding line reconstruction from Bentley et al. (2014) (thick black lines) are compared to simulated grounding line retreat in one of the ensemble members for the Last Interglacial (LIG, red line). Regions previously identified as potentially viable for Oldest Ice (Van Liefferinge and Pattyn, 2013) are outlined in black. Eight ice core locations are highlighted, which are used as tuning targets with respect to ice core thickness and analysed in Figure 7 (West Antarctica) and 8 (East Antarctica), respectively.

Feldmann et al., 2014) to allow for reversible grounding line migration despite relatively coarse resolution. Basal sliding is calculated with a pseudo-plastic sliding law (Schoof, 2010) in which the yield stress (τ_c) is determined by the pore water

content and the strength of the sediment which is set by a linear piecewise function dependent on the ice-bedrock interface depth relative to sea level. Through this heuristic parameterisation marine-based ice has a more slippery base as compared to ice above sea level, allowing for faster flowing marine outlet glaciers. The parameter space used here yields a basal friction coefficient e.g. underneath Thwaites glacier on the lower end compared to Yu et al. (2018). Since the simulations presented here span a long time frame (2 MA), we abstain from the derivation of basal friction by inversion (optimization problem) as we want to prevent over-tuning of present-day flow patterns. All simulations are carried out on a 16x16 km^2 grid and 81 vertical levels with refined resolution near the base (≈ 18 m at the ice-bedrock interface). The grid resolution resolves the major ice streams while allowing for reasonable computation times, yet small outlet glaciers such as in the Antarctic Peninsula cannot be simulated adequately on this resolution.

The initial topography used for the simulations consists of a 200 ka thermal spinup of the BEDMAP2 (Fretwell et al., 2013, see Figure 1) data set (present day steady state simulation with fixed ice sheet geometry), refined around LDC and Dome Fuji by the new radar derived topographies published in Young et al. (2017) and Karlsson et al. (2018). As basal heat flux is crucial for the existence of 1.5 Myr old ice (Fischer et al., 2013; Van Liefferinge and Pattyn, 2013) as well as for ice dynamics, especially in the interior ice sheet (Larour et al., 2012), we consider four different geothermal heat flux (GHF) datasets (Shapiro and Ritzwoller, 2004; Purucker, 2013; An et al., 2015; Martos et al., 2017) in our simulations to account for uncertainties in GHF and to illustrate their impact on ice dynamics and potential Oldest Ice candidate sites.

Sea level plays an important role in the stability of marine ice sheets as it affects the position of the grounding line via the floatation criterion. We employ three different sea level reconstructions to account for different glaciation patterns in the northern hemisphere and different sea level highstands in Interglacials. PISM does not account for self-gravitational effects yet, which can have a stabilising effect on the ice sheet locally in Interglacials (Konrad et al., 2014). Ice shelf melt rates are calculated based on the parameterisation in Beckmann and Goosse (2003), with a square dependency on the temperature difference between the pressure dependent freezing point and the ambient ocean temperature as used in e.g. Pollard and DeConto (2012). The ambient ocean temperature is derived from simple extrapolation of the 3D ocean temperature into the ice shelf cavity. Recently, there have been developments towards more realistic representations of basal shelf melt in standalone continental ice sheet models, incorporating sub-shelf ocean circulation (e.g. Reese et al., 2018; Lazeroms et al., 2018) which improve the representation of basal ice shelf melt rates, but they have not been included in this study. To better match present day observed sub ice-shelf melt rates (Rignot et al., 2013; Depoorter et al., 2013), we linearly scale the computed present day melt rates in the Amundsen and Bellinghausen Sea by a factor of 10 and underneath the Filchner Ice Shelf by a factor of 1.5. Shelf melt rates adjacent to Wilkes, Terre Adelie and George V Land in East Antarctica are also scaled by factor of 10. These scaling factors are kept constant throughout the paleo simulations. Ice shelf calving and therefore the dynamic calving front is derived via two heuristic calving parameterisations: 1. thickness calving (cH) sets a minimum ice thickness (75 m or 150 m) at the calving front, if the ice thickness drops below this threshold, ice in the respective grid node is purged; 2. Eigencalving (cE) calculates a calving rate from the ice shelf strain rates (Albrecht and Levermann, 2014).

2.2 Climate Forcing

To adequately capture continental ice sheet dynamics on long timescales (i.e. millennia and more), in principle, a coupled modelling approach is required to resolve climate-ice sheet interactions. First efforts to tackle multi-millennial timescales via a fully coupled modelling approach are promising and currently being developed (e.g. Tigchelaar et al., 2018). However, coupled

5 climate-ice sheet models which resolve ice shelf-ocean interactions are mostly limited to applications on the centennial time scale due to computational limitations. To bridge this shortcoming, we construct a transient climate forcing over the last 2 Myr by expanding time-slice snapshots from the Earth system model (ESM) COSMOS (Lunt et al., 2013) with the glacial index method as applied in Sutter et al. (2016). The climate snapshots are based on Pliocene (Stepanek and Lohmann, 2012), LIG (Pfeiffer and Lohmann, 2016), LGM and Pre-Industrial orbital, atmospheric and topographic conditions. For each climate

10 snapshot, anomaly fields with respect to the pre-industrial control run are calculated and added to a mean Antarctic climatology (1979-2011) from the regional climate model RACMO (van Wessem et al., 2014), or the extrapolated World Ocean Atlas 2009 (Locarnini et al., 2010) to provide the climate forcing for the individual climate epoch. The intermediate climate states between the snapshots are calculated by interpolating the anomaly fields with a glacial index approach, utilizing either of two glacial indices (see Figure 5 middle panel) derived from the Dome C deuterium record from Jouzel et al. (2007) which is expanded to

15 the last 2 million years by a transfer function (Michel et al., 2016) using the marine sediment core from Lisiecki and Raymo (2005) or the global data set from Snyder (2016). The forcing variables (surface temperature T_s, ocean temperature T_o) can then be calculated at every grid point in time by:

$$T_s^{i,j}(t) = T_{spd}^{i,j} + \sum_{x=\mathrm{ig,g,p}} \omega_x(t)\hat{T}_{s_x}^{\,i,j} \tag{1}$$

$$T_o^{i,j,z}(t) = T_{opd}^{i,j,z} + \sum_{x=\mathrm{ig,g,p}} \omega_x(t)\hat{T}_{o_x}^{\,i,j,z} \tag{2}$$

20   where subscript i,j denotes the grid point, z denotes the depth of the ice ocean interface at grid point (i,j), $T_s^{i,j}(t)$ is the surface temperature at grid point i,j at time t, $T_{opd}^{i,j}$ is the surface temperature at present day (mean climatology from 1979-2016), $\hat{T}_{s_{ig}}^{\,i,j}$ is the ESM anomaly at the LIG $\hat{T}_{s_g}^{\,i,j}$, LGM $\hat{T}_{s_p}^{\,i,j}$, and in the Pliocene, respectively. The linear scaling factors $\omega_x(t)$ are derived from the glacial index (GI) which interpolate the climate forcing at any given time between the respective climate states. The scaling $\omega_x(t)$ is computed by

$$\omega_g(t) = 1.0 - \frac{max(\mathrm{GI}, \mathrm{GI}_{\mathrm{pd}})}{\mathrm{GI}_{\mathrm{pd}}}) \begin{cases} 1.0 \ \mathrm{for} \mathrm{GI} = 0.0 \\ 0.0 - 1.0 \ \mathrm{for} \ 0.0 < \mathrm{GI} < \mathrm{GI}_{\mathrm{pd}} \\ 0.0 \ \mathrm{for} \mathrm{GI} \geqslant \mathrm{GI}_{\mathrm{pd}} \end{cases} \tag{3}$$

$$\omega_{ig}(t) = \frac{(max(\mathrm{GI}, \mathrm{GI}_{\mathrm{pd}}) - \mathrm{GI}_{\mathrm{pd}})}{(1.0 - \mathrm{GI}_{\mathrm{pd}})} \begin{cases} 1.0 \ \mathrm{for} \mathrm{GI} = 1 \\ 0.0 - 1.0 \ \mathrm{for} \ \mathrm{GI}_{\mathrm{pd}} \leqslant \mathrm{GI} \leqslant 1.0 \\ 0.0 \ \mathrm{for} \mathrm{GI} \leqslant \mathrm{GI}_{\mathrm{pd}} \end{cases} \tag{4}$$

$$\omega_p(t) = \frac{(max(\mathrm{GI}, 1.0) - 1.0)}{(1.0 - \mathrm{GI}_{\mathrm{pd}})} \begin{cases} 1.0 \ \mathrm{for} \mathrm{GI} = \mathrm{GI}_{\mathrm{max}} \\ 0.0 - 1.0 \ \mathrm{for} \ 1.0 \leqslant \mathrm{GI} \leqslant \mathrm{GI}_{\mathrm{max}} \\ 0.0 \ pd for GI \leqslant 1.0 \end{cases} \tag{5}$$

where the subscripts pd, ig and p stand for Glacial, Interglacial and Pliocene respectively and GI_{pd} refers to the present
day glacial index. The major difference between the two glacial indices is the warmer overall climate state recorded in Snyder
(2016) before the MPT (see Figure 5 b). The present day forcing derived from van Wessem et al. (2014) matches the present
day climatology in Antarctica (compared to in-situ measurements) very well, with biases in the high antarctic plateaus of less
than 5%.

We apply a temperature dependent scaling of precipitation (P), using a scaling factor (percent precipitation change per
degree Celsius) of α_P of 3, and 5 %, respectively, motivated by central East Antarctic paleo precipitation changes (Frieler
et al., 2015; Werner et al., 2018),

$$P(t) = P_{pd} + (T_{spd}^{i,j} - T_s^{i,j}(t))\alpha_P \tag{6}$$

but underestimating sensitivity of coastal mass balance to temperature changes.

In this standalone approach, the Antarctic Ice Sheet (AIS) is responding to the external forcing, thus no feedbacks are acting
between the ice sheet and the climate system. However, the glacial index approach implicitly incorporates the integrated climate
response to changes in orbital configuration and atmospheric CO_2 archived in the Dome C (Jouzel et al., 2007), the marine
sediment core (Lisiecki and Raymo, 2005) or the global air temperature (Snyder, 2016) record. This allows to investigate the
dynamical response of the AIS to a shifting climate regime across the MPT, with the caveat, that ice sheet–climate interactions
which are not included in the GCM time slice approach might have also played a significant role in the ice sheet evolution
during the MPT transition.

2.3 Model ensemble approach

To address the multitude of uncertainties regarding the paleoclimate state during the last 2 million years, the applied boundary
conditions and the physics of ice flow, we choose a model ensemble approach. The aim of the ensemble design (Figure 2) is to
investigate the impact of different climate forcings, the response of the AIS to different geothermal heat flux signatures (Figure

5   3) and the impact of sea level (Figure 5, bottom panel) on the transient configuration of marine ice sheets. Ultimately, different
manifestations of ice sheet flow and climate response are investigated via a set of ice sheet model parameterisations (Table
2). The model parameters are pre-selected in equilibrium simulations under present day forcing (1979–2011 climatology from
van Wessem et al. (2014) and World Ocean Atlas (Locarnini et al., 2010) ocean temperatures) trying to fit the current sea level
equivalent ice sheet volume, geometry, ice flow, ice thickness at selected ice core locations (Figure 1), as well as the Antarctic

10 sea level contribution during the last two glacial cycles. The ensemble is built around two main branches of ensemble runs
consisting of a set of boundary conditions (Table 1) and ice sheet model parameterisations (Table 2).   In the first ensemble
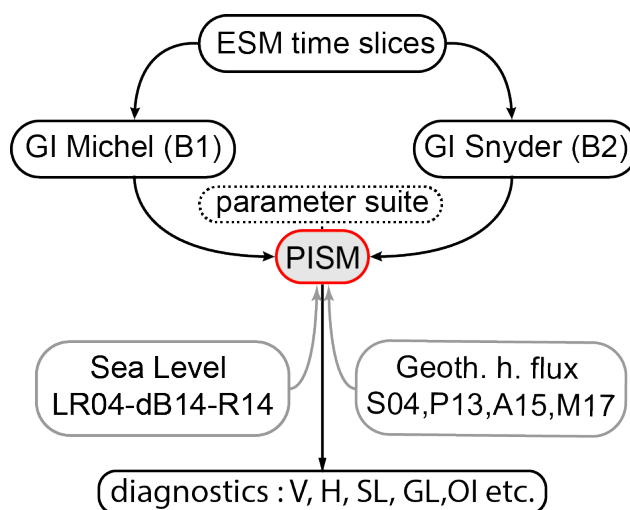
Figure 2. Schematic flow chart of model ensemble. The ice sheet model (PISM) is forced via the transient forcing derived by linear interpo-
lation with glacial indices from Michel et al. (2016) and Snyder (2016) forming ensemble branch B1 and B2. Prescribed input data consist
of sea level (SL) data and geothermal heat flux (GHF) data sets. The parameter suite is derived from sensitivity studies in which the present
day Antarctic Ice Sheet and its sea level contribution during the last two glacial cycles were the main tuning targets.

branch (B1) the glacial index is derived from an extrapolation of the EPICA Dome C temperature record (Jouzel et al., 2007)
via correlation to the Lisiecki and Raymo (2005) time series to span the last two million years (Michel et al., 2016). In the
second branch (B2) the glacial index is derived from the global air temperature record in Snyder (2016). Major differences

15 between 2–0.9 Myr BP can be identified in the two resulting glacial indices. B2 exhibits much warmer climate conditions be-
tween 2–1.2 Myr ago. The warmest climate state in B1 is the ESM time slice centred in the LIG (MIS5) (Pfeiffer and Lohmann,
2016) while in B2 the Interglacials between 2 and 1.7 Myr BP are the warmest, represented by a middle Pliocene climate time
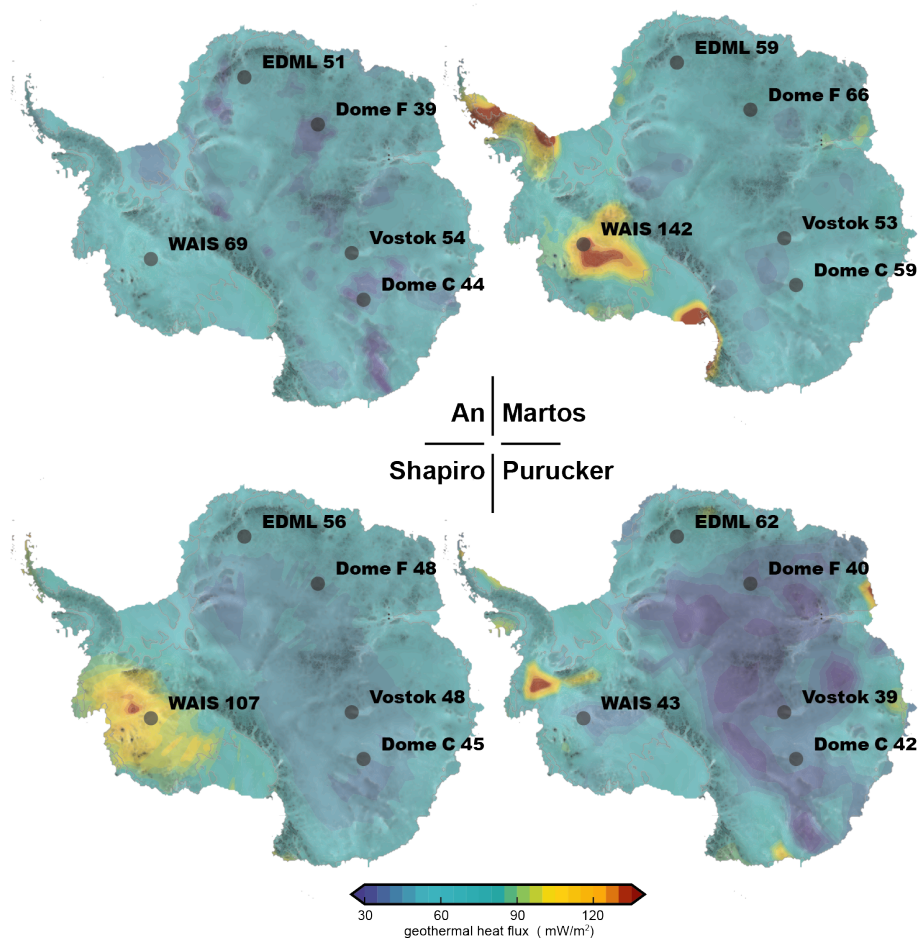
Figure 3. The four panels illustrate the four GHF input data sets (Shapiro and Ritzwoller, 2004; Purucker, 2013; An et al., 2015; Martos et al., 2017) used in this study. As a reference the rounded GHF (in $\mathrm{mW/m2}$) at selected ice core locations is provided.

Table 1. Available choices of selected forcing fields for the model ensemble. B1 and B2 stand for the two glacial indices derived from Michel et al. (2016) and Snyder (2016); SL data from Lisiecki and Raymo (2005) (LR05), de Boer et al. (2014) (dB14),Rohling et al. (2014) (R14); GHF data from Shapiro and Ritzwoller (2004) (S04), Purucker (2013) (P13), An et al. (2015) (A15), Martos et al. (2017) (M17).

Forcing	GI	SL	GHF
Data	B1, B2	LR05,dB14,R14	S04,P13,A15,M17

slice (Stepanek and Lohmann, 2012) (see Figure 5, middle panel).

8

Table 2. Selected ISM parameters for the model ensemble. cH stands for thickness calving limit (in meter), cE is a parameter in the Eigen-calving equation. $\text{till}_{\min}$ and $\text{till}_{\max}$ modify basal friction in the sliding law. γ_{EAIS} is a dimensionless scaling factor for basal shelf melt for selected East Antarctic ice shelf regions (George V Land, Wilkes Land).

Parameter	sia	ssa	cH (m)	cE	$\text{till}_{\min}$	$\text{till}_{\max}$	γ_{EAIS}
Values	1.0 ; 1.7 ; 2	0.55 ; 1.0	75 ; 150	$1 \cdot 10^{17}$	5 ; 10	30 ; 40	1 ; 10

3 Results & Discussion

The main objective of this work is to assess the existence of 1.5 Myr old ice along the East Antarctic ice divide. We simulate the ice dynamics throughout the last 2 MA, focussing on ice volume changes specifically across the MPT (see Figure 5), ice sheet configurations in Glacials (focussing on marine isotope stage 2) and Interglacials (with a focus on marine isotope stage 11 and 5, see Figure 6), ice thickness changes at ice core locations in West and East Antarctica (see Figure 1) and conclude with a map of promising sites providing suitable conditions for an Oldest Ice ice core around Dome Fuji, Dome C and Ridge B, following the approach of Fischer et al. (2013) and Van Liefferinge and Pattyn (2013).

3.1 Antarctic ice volume changes

We divide our discussion of the evolution of AIS volume into three time frames: 1. pre-MPT (2 – 1.2 Myr BP), MPT (1.2 – 0.9 Myr BP), and post-MPT (0.8 – 0 Myr BP). To put our results into perspective, we compare them to two published transient ice sheet model studies which cover the time interval considered here (Pollard and DeConto (2009) and de Boer et al. (2014)) as well as Tigchelaar et al. (2018), which spans the last 0.8 MA. Figures 4 and 5 depict the transient evolution of AIS volume as simulated by the whole ensemble and a representative subset of our model ensemble in comparison to Pollard and DeConto (2009), de Boer et al. (2014) and Tigchelaar et al. (2018) and with respect to different choices of GHF and glacial index. In Figure 5 we present two clusters of the model ensemble from branch B1 (ice/marine sediment core glacial index) and the branch B2 (global air temperature glacial index). Depicted are three simulations from both B1 and B2 with identical model parameterisations using three different GHF data sets (Shapiro and Ritzwoller, 2004; Purucker, 2013; Martos et al., 2017).

3.1.1 pre-MPT Antarctic Ice Sheet dynamics

Simulated ice volume changes before the MPT are characterised by a strong obliquity (≈ 41 m) cycle resembling the glacial index forcing which is formed by the integrated planetary response to orbital variations. The two clusters in the upper panel of Figure 5 show a present day ice sheet configuration (B1-branch) and a strong interglacial configuration in which the WAIS is collapsed (B2-branch). Note that most of the ensemble members do not allow a significantly increased glaciation as encountered during the last 800 ka. Maximum AIS volume increase during the pre-MPT phase is limited to less than 2-4 m sea level equivalent ice volume throughout the model ensemble. Variability in the B2-branch is higher than in B1, resembling the waxing and waning of the marine West Antarctic Ice Sheet (WAIS) and stronger Glacial–Interglacial surface mass balance
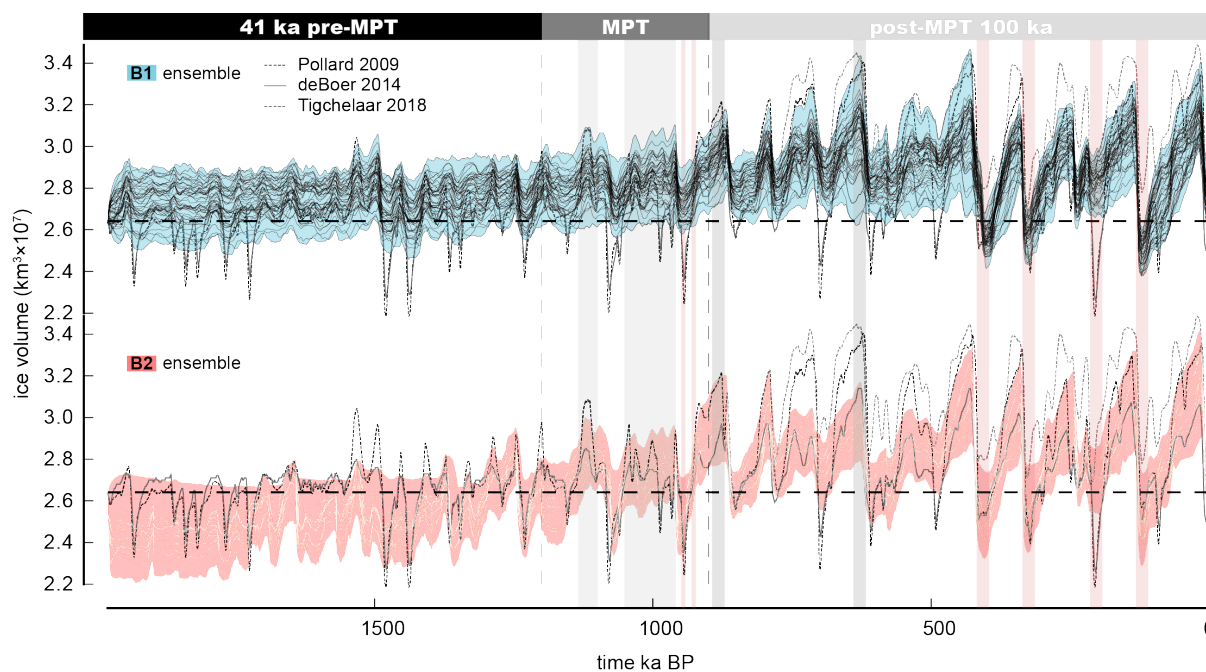
Figure 4. Antarctic ice volume as simulated in the full model ensemble (excluding simulations with either present day ice volume larger than $2.8 \cdot 10^7$ km^3 or Last Glacial Maximum ice sheet volume smaller than $3.0 \cdot 10^7$ km^3). Black dashed line denotes present day ice volume derived from BEDMAP2 (Fretwell et al., 2013).

variability. Ice volume in the B1-branch is predominantly driven by surface mass balance and sea level. The comparison to Pollard and DeConto (2009) and de Boer et al. (2014) illustrates the imprint of the different forcing approaches. While Pollard and DeConto (2009) and de Boer et al. (2014) derive the climate forcing directly from the orbital configuration, we construct a transient climate forcing by combining ESM snapshots from the Pliocene, LIG and LGM with a glacial index.

5 This apparently leads to more muted responses to interglacial conditions during the pre-MPT and a generally lower variability (sea level equivalent of ca. $4 - 8$ m), while the growth and retreat phases are more or less synchronous to the variations in Pollard and DeConto (2009) and de Boer et al. (2014). One main similarity between our study and the results from Pollard and DeConto (2009) and de Boer et al. (2014) is that the East Antarctic Ice Sheet (EAIS) margins are relatively stable throughout the pre-MPT.

10 3.1.2 MPT Antarctic Ice Sheet dynamics

Commonly, the onset of the MPT is put at 1.2 Myr BP and ends about 0.9 Myr BP culminating in the extended cold conditions between marine isotope stages 24 and 22 (ca. 940-880 ka BP). Two pronounced Interglacials (MIS31 and MIS25) and several "lukewarm" events (between 1050 ka and 950 ka BP) separated by moderate glacial conditions throughout the MPT can be identified in the glacial index forcing (Figure 5 panel b). The AIS response during the MPT is dominated by two proto-glacial
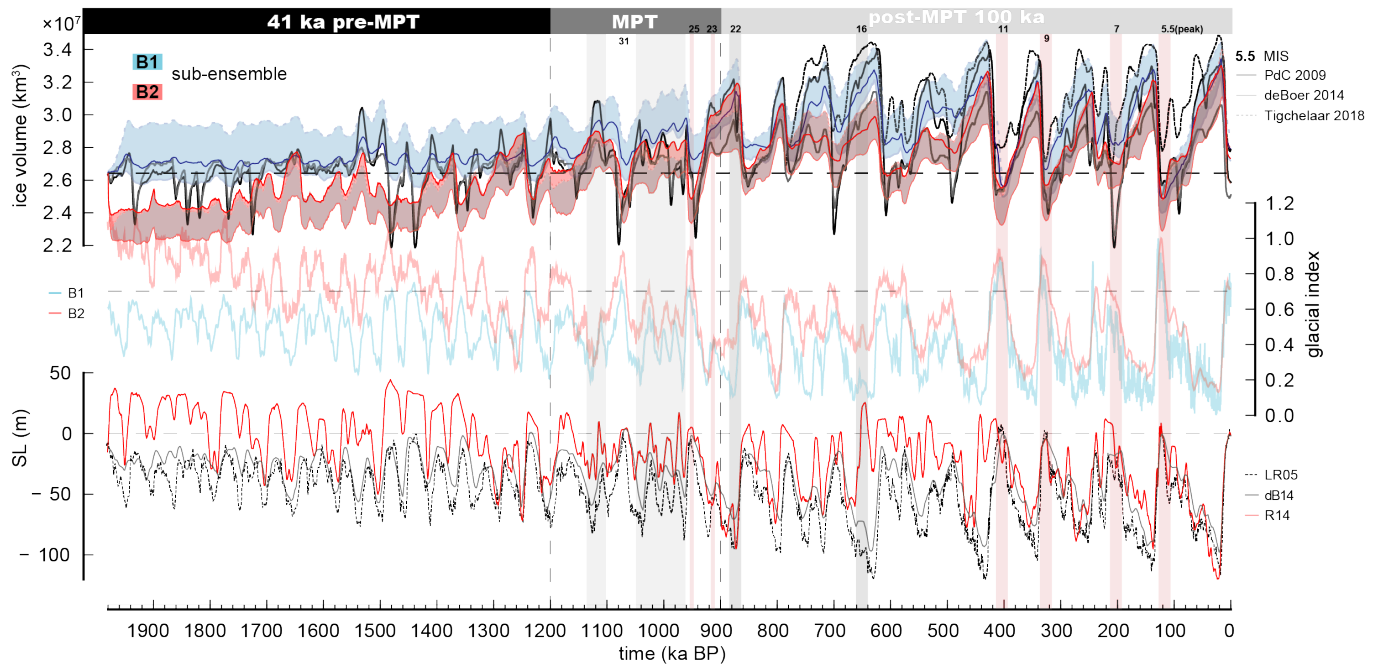
Figure 5. Upper panel depicts the ice volume evolution of a subset of the model ensemble. Blue and light blue curves depict ensemble branch B1 with parameters: sia 1.0; ssa 0.55; till$_{min/max}$ 5/10; cH 75; cE $1e^{17}$; γ_{EAIS} 20; SL LR04. Geothermal heat flux for blue curve (Shapiro and Ritzwoller, 2004) upper light blue dashed (Purucker, 2013), lower light blue (Martos et al., 2017). The red curves show B2 with identical parameters but glacial index from Snyder (2016) including Pliocene climate forcing. Red (Shapiro and Ritzwoller, 2004), dashed maroon (Martos et al., 2017), maroon (Purucker, 2013)). The simulated ice volume from Pollard and DeConto (2009); de Boer et al. (2014); Tigchelaar et al. (2018) are shown for comparison (black, gray and black dashed line). The middle panel shows the glacial index used in B1(dark grey) and B2 (light gray) with gray dashed line depicting average Holocene index. The lower panel shows the sea level reconstructions used in the model ensembles ((Lisiecki and Raymo, 2005, LR04), (de Boer et al., 2014, dB14), (Rohling et al., 2014, R14)).

states between 1.1 – 1.0 Myr BP separated by interglacial MIS31 which can be interpreted as a first expression of a 100 ka cycle. However, obliquity pacing still dominates ice dynamics at this stage. The second proto-glacial state after MIS31 is interupted by MIS25 followed by an extended cold period, allowing for the formation of marine ice sheets in the Weddell and Ross Seas similar to what is observed during late Quaternary Glacials, marking the end of the MPT and the onset of unperturbed 80-120

5 ka cycles in AIS volume. Our ice sheet model results are in line with the notion of a 900-ka event by Elderfield et al. (2012), which is centred around MIS25-22, manifesting in a qualitative difference in the formation of Glacials: a long build up phase ended by a sharp decline of the ice volume into Interglacials (late Quaternary sawtooth pattern) during the last 800 ka and a more symmetric glaciation/deglaciation before the MPT. We find no evidence of large changes in the EAIS margin during the MPT as proposed by Raymo et al. (2006). However, most simulations from B2 which include warm Pliocene climate

10 conditions show a major re-organisation of West Antarctica into a "present day" ice sheet configuration at the end of the MPT (see Figure 7). This might represent a West Antarctic pendant to the theory that the EAIS transitioned to a marine configuration

during the MPT (Raymo et al., 2006), which does not require significant changes in the EAIS margin during the MPT. Such a configurational WAIS-shift would potentially implicate strong climate feedback mechanisms due to the formation of an ocean gateway between the Weddell, Ross and Amundsen Sea (Sutter et al., 2016) affecting climate dynamics across the MPT. This transition is not simulated in B1 and calls for a more crucial analysis outside the scope of this publication, e.g. incorporating a

5 fully coupled ESM with a dynamical ice sheet component. Accordingly, the climate state in B1 does not allow a waxing and waning of the WAIS for pre-MPT interglacial conditions. We note, that other modelling studies either focussing on warmer Pliocene stages (DeConto and Pollard, 2016) or regional sensitivity studies (Mengel and Levermann, 2014) show large scale retreat of the grounding line into the Wilkes and Aurora subglacial basins, therefore a potential re-organization of the EAIS across the MPT cannot be excluded. The hypothesis of a dynamic marine EAIS margin during the MPT is a very promising

10 target for continental transient ice sheet modelling in concert with findings from the aspired Oldest Ice ice core. The end of the MPT is marked by a pronounced glacial state at MIS 22 akin to the Last Glacial Maximum reflecting a strong growth of the AIS at the end of the MPT. This results is robust across all ensemble members for both branch B1 and B2. It is interesting to note that the glaciations in the MPT interval become progressively stronger and reach a full late Quaternary glaciation state in MIS 22.

15 ### 3.1.3   post-MPT Antarctic Ice Sheet dynamics

The simulated Quaternary AIS volume evolution can be roughly divided into two parts, the first spanning the window from 900 ka BP to 420 ka BP (MIS11) and the second from MIS11 to today. After MIS 11 ice volume variability increases with smaller interglacial and bigger glacial ice sheets compared to the preceeding 500 ka. This pattern mostly reflects the stronger interglacial atmospheric and ocean temperature forcing from MIS11 onwards. MIS 11 is the first late Quaternary interglacial

20 in which the WAIS recedes to a land based ice sheet configuration in B1 with the second major interglacial being MIS5e. The ensemble mean sea level contribution in MIS5e amounts to $\approx 2.5 - 3$ m with a full ensemble range between 1 and 4.5 m (see Figure 6). Glacial ice volume in the late Quaternary grows to ca. -8 to -10 m sea level equivalent ice volume (see Figure 3) with strongest Glacials represented by MIS16 and 2. The different forcing approaches of our study and Pollard and DeConto (2009); de Boer et al. (2014) and Tigchelaar et al. (2018) are apparent e.g. in the largest ice sheet retreat ocurring

25 in our ensemble at MIS5e while located at MIS 7 (ca. 210 ka BP) for both Pollard and DeConto (2009) and de Boer et al. (2014) while in Tigchelaar et al. (2018) Quaternary ice sheet volume never drops below the present AIS volume. Note also, that the stability of the marine WAIS is crucially dependent on the choice of the GHF, as all simulations with the GHF field from Purucker (2013) exhibit a collapse of the WAIS in the LIG with a much smaller percentage for both Martos et al. (2017) and Shapiro and Ritzwoller (2004). In our simulations, the applied sea level forcing plays a minor role in the stability of the

30 WAIS in lnterglacials (not shown).

3.2   The role of geothermal heat flux

It is a well established fact, that the heat flux at the ice-bedrock interface can be a major driver of ice sheet dynamics. Albeit, GHF for the Antarctic Ice Sheet is poorly constrained (Martos et al., 2017) and the few published continental data sets available
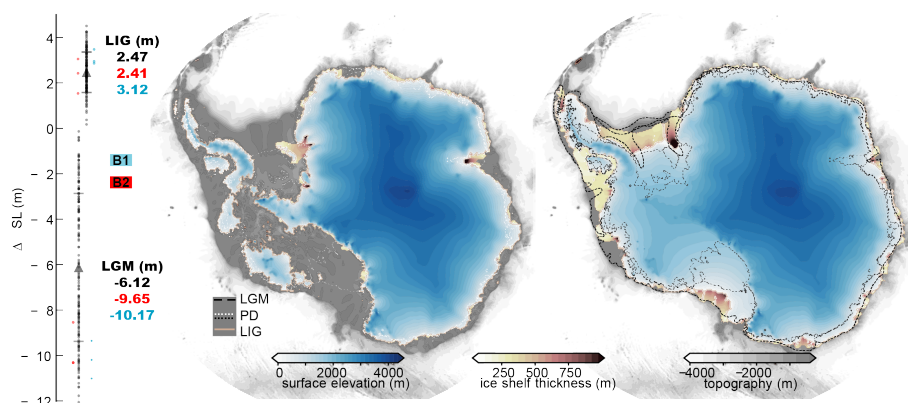
Figure 6. Left panel shows simulated ice volume equivalent global sea level change in the LIG and LGM for the whole ensemble (black dots), with mean sea level contribution (black triangle) and standard deviation (black bars). Ensemble members depicted in Figures 5,7 and 8 are shown in blue (B1) and red (B2). Middel and left panel illustrate simulated ice sheet configurations for the LGM and Last Interglacial. Reconstructed grounding line positions for the LGM (Bentley et al., 2014) and BEDMAP2 (Fretwell et al., 2013) are depicted for comparison.

differ substantially (see Figure 3 and Martos et al. (2017)). We can analyse the impact of GHF in our model ensemble by gauging the fit of diagnostic variables (ice thickness, basal melt, basal temperature, ice volume) in comparison to observed data. Both data sets from Purucker (2013) and An et al. (2015) show relatively low heat flux along the East Antarctic ice divide and overall for the West Antarctic Ice Sheet. In consequence, potential "Oldest Ice" candidate sites indicated by the model

5   ensemble and using those two data sets are unrealistically large (see Figure 9), specifically for the Dome Fuji region. This is the case regardless of the model parameterisation and climate forcing or sea level input data. The choice of geothermal heat flux imprints on both East and West Antarctic ice dynamics, while mostly modulating ice thickness (leading to thickness changes of up to 20%) in East Antarctica but also impacting the simulated ice divide along the transect of Dome A-Ridge B-Vostok-Dome C (see Figure 9). The impact of heat flux in West Antarctica can be drastic, as it acts as a major control on the marine ice sheet

10   instability. Overall ice sheet variability between ensemble members (for identical parameter settings) due to different choices of GHF is consistently larger than due to the choice of different sea level forcing. This emphasises the strong role of GHF in modulating Antarctic Ice Sheet dynamics and overall evolution of ice volume.

3.3 Ice thickness variability in WAIS and EAIS

Ice thickness is an important parameter controlling the viability of a continuous 1.5 million year old ice core record at a given

15   location. If the ice is too thick, its insulating properties lead to melting at the ice bedrock interface, if it is too thin, either old ice is transported away too quickly or the layering might be too thin to decipher a meaningful transient climate signal. Figures 7 and 8 show the ice thickness change at the four East and West Antarctic ice core locations (depicted in Figure 1).
In the simulations with a collapsed late Pliocene WAIS, the MPT leads to the advance of the WAIS into a present day configuration going along with a closure of the open ocean connection between the Weddell-, Amundsen/Bellinghausen- and Ross-Seas.
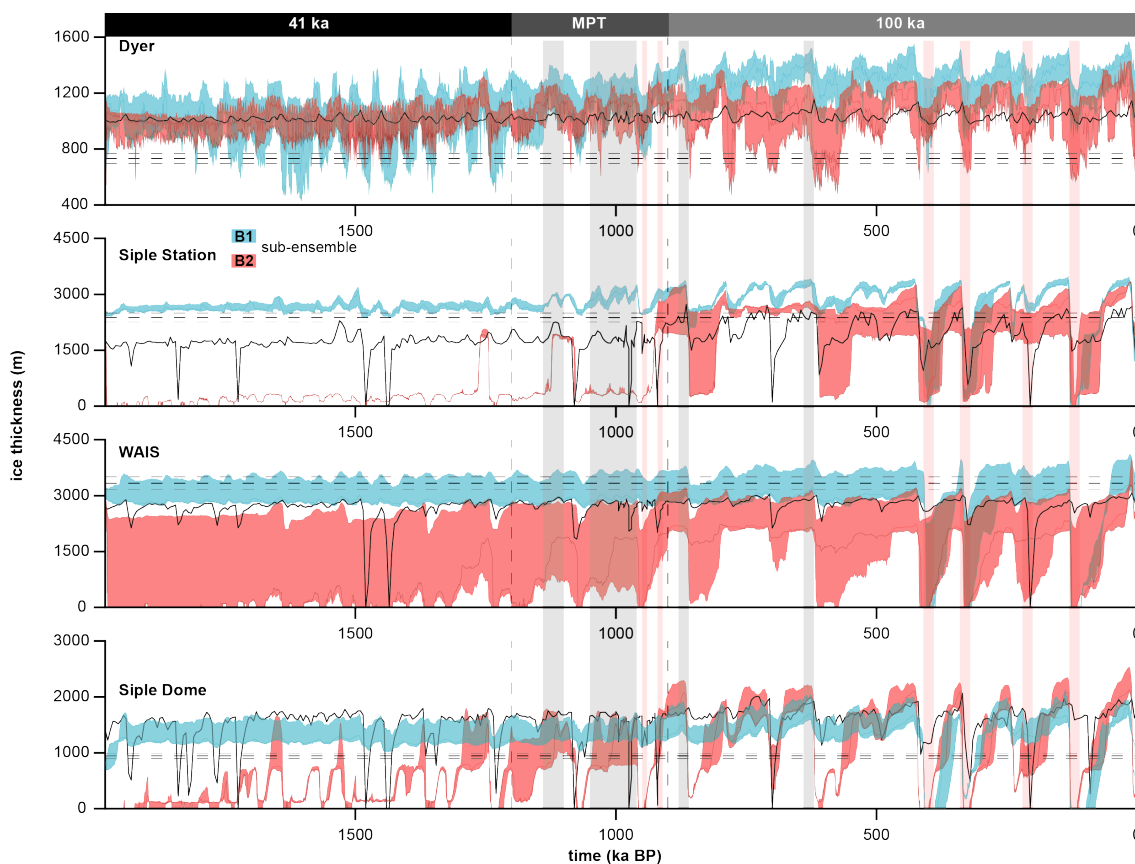
Figure 7. Ice thickness evolution during the last two Myr as simulated in our model ensemble for the four West Antarctic ice core locations (see Figure 1). Blue lines are from ensemble B1 (as in Figure 5) red lines from B2. Sampling rate is 1 ka. For comparison, the ice thickness evolution simulated in Pollard and DeConto (2009) is plotted in black (sampling rate 10 ka). The observed present day ice thickness, derived from BEDMAP2 (Fretwell et al., 2013), is shown by the black dashed line, with 5% variation illustrated by grey dashed lines. The ice thickness simulated in Pollard and DeConto (2009) is from a 5 Myr transient simulation using BEDMAP1 (Lythe et al., 2001) as the initial ice sheet configuration.

However, in those simulations with no early Pleistocene WAIS, the WAIS remains relatively small throughout the Quaternary which is likely to be an indication that the climate forcing is too warm.

5   The ensemble members with a stable interglacial pre-MPT WAIS transition to a higher variability during the MPT with no major re-organisation of ice flow and grounding line dynamics. Changes in the EAIS manifest in an increase in ice thickness variability by ca. 30%. The shift to larger Glacial–Interglacial ice thickness changes is evident at all ice core locations and mostly due to the more pronounced climate cycles following the MPT. The temporal evolution of ice thickness changes for the different East Antarctic ice core locations follows a similar pattern with muted variability during the pre-MPT and a

14
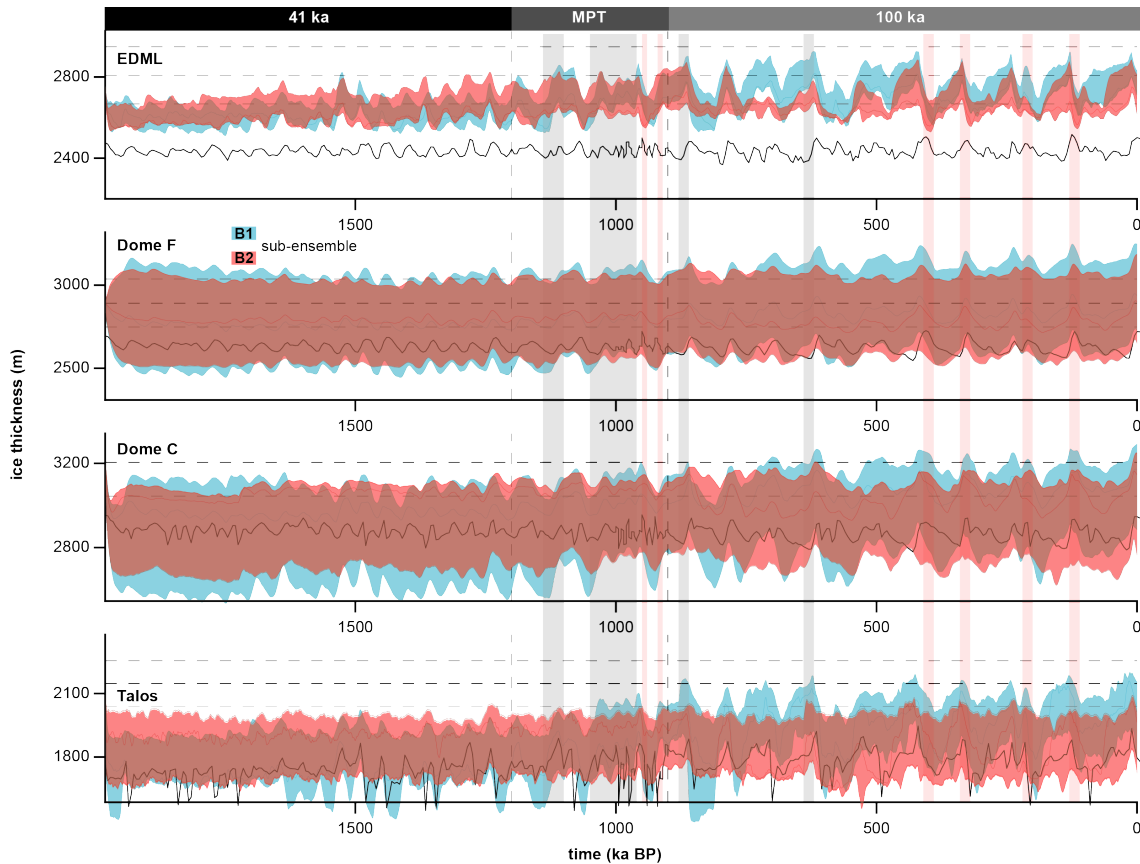
Figure 8. Same as Figure 7 but for the four East Antarctic ice cores.

gradual increase completed by ca. 900 ka BP. Note, that we find different points in time regarding ice thickness maxima for the central dome positions Dome C and Dome Fuji compared to positions away from the central Domes such as around the EDML and Talos Dome ice cores. While the former generally show ice sheet maxima during mid Interglacials, the latter show maxima generally at the onset of Interglacials and declining ice thicknesses during the Interglacial. This and the higher variability for the two coastal locations (EDML and Talos) can be explained by the impact of grounding line migration and larger Glacial–Interglacial surface mass balance differences. Mean ice thickness variability for Dome Fuji and Dome C during the late Quaternary is 165 and 195 m, respectively (105 and 140 during pre-MPT). Overall, the simulated present day ice cover after 2 million years at the highlighted ice core locations is in good agreement (within $\approx 5\%$) with the BEDMAP2 (Fretwell et al., 2013) data set.

3.4 Mapping potential Oldest Ice sites

We apply the conditions for the existence of 1.5 Myr old ice derived in Fischer et al. (2013) to our simulations in order to investigate the impact of the transient paleo-climate forcing, GHF and different model parameterizations on the sites Dome

Fuji, Dome C and Ridge B (Figure 9). We identify similar Oldest Ice regions as in Van Liefferinge and Pattyn (2013); Van Liefferinge et al. (2018); Parrenin et al. (2017); Passalacqua et al. (2017). This gives us confidence in the robustness of our model results and shows, that the transient forcing and continental setup used here does not change the general conclusions in Van Liefferinge et al. (2018). The regions with major overlaps to Van Liefferinge et al. (2018) are thus promising sites from a

5 paleo ice-climate dynamics viewpoint as well as from the detailed dissection of the present day conditions. Overall, applying the GHF from the data set by Shapiro and Ritzwoller (2004) yields the best agreement with the findings of Van Liefferinge and Pattyn (2013); Van Liefferinge et al. (2018); Parrenin et al. (2017) and Passalacqua et al. (2017). However, the geothermal heat flux data set from Martos et al. (2017) matches the observed/derived heat flux at Dome C to a better degree. In the simulations with the Martos et al. (2017) data set, the present day ice divide around Dome C is shifted strongly (ca. 160 km) in direction of

10 the Ross Sea/Belgica Subglacial Highlands compared to the other three data sets due to the low geothermal heat flux south-east of the Dome C region contrasting with the high heat flux around Dome C. Simulations using the Martos et al. (2017) data set show almost no viable conditions for the existence of Oldest Ice in East Antarctica (with the exception of oldest ice patches around Dome A, Ridge B and in the Belgica Subglacial Highlands east of Dome C), as basal temperatures are relatively high due to the large heat flux at the base of the ice leading to sustained basal melting. This is the case despite the relatively low

15 ice thickness (and therefore insulation) simulated with the Martos et al. (2017) data set. Simulations with the Purucker (2013) and An et al. (2015) GHF reconstruction overestimate the Oldest Ice area substantially (showing viable conditions also for the Dome Fuji and Dome C ice core location). Interestingly however, the Purucker (2013) data sets yields best agreement between the simulated and observed present day ice divide for Dome Fuji as well as Dome C. The effect of the geothermal heat flux forcing is not limited to the basal temperature of the ice, but also has a substantial impact on overall ice thickness (up to 20%

20 see Figure 8).

Our findings indicate, that the existence of Oldest Ice is not only dependent on the choice of GHF but can also be influenced by the applied climate forcing or ice flow parameterisation modulating the regions illustrated in Figure 9. Despite regional differences all three sites (Dome Fuji, Dome C, Vostok/Ridge B) show suitable conditions for an Oldest Ice core throughout

25 the last 1.5 Myr for ensemble members using either the GHF from Shapiro and Ritzwoller (2004) or Purucker (2013) and An et al. (2015) (see Figure 9). However the later two show unreasonably large Oldest Ice patches. While both LDC and North Patch (Parrenin et al., 2017) are identified in our model results, the regions of Oldest Ice at Dome Fuji are somewhat shifted in comparison to the findings in (Van Liefferinge and Pattyn, 2013; Van Liefferinge et al., 2018). This might be due to the different input data or ice dynamics simulated, or affected by differences in resolution or the thermal state at the base of the ice.

30 However, the generally robust agreement between high resolution studies (Van Liefferinge et al., 2018; Parrenin et al., 2017; Passalacqua et al., 2017) and our coarse resolution paleo dynamics approach strengthens the notion of viable conditions for Oldest Ice both at Dome Fuji and Dome C as well as Ridge B.

4 Conclusions

The search for the major drivers of the mid Pleistocene transition is ongoing, with ice sheets acting as a crucial component of climate system re-arrangement. Our model ensemble simulations indicate both rapid transitions and gradual growth of the Antarctic Ice Sheet during the MPT, featuring the buildup of a large glacial ice mass in West Antarctica driven by extended glacial conditions and muted Interglacials between 1.2 and 0.9 Myr BP. These findings fit well to the notion of a significant expanse of the Antarctic Ice Sheet around 0.9 Myr BP by Elderfield et al. (2012). However, we do not find a major re-organisation of the EAIS grounding line across the MPT which is in contrast to the theory that the EAIS transitioned from a mostly land based ice sheet to a marine configuration (Raymo et al., 2006) in this interval. However, such a re-organisation cannot be excluded at this point, as several other modelling studies show potential phases of major EAIS grounding line retreat in the Pliocene or under strong interglacial conditions (DeConto and Pollard, 2016; Mengel and Levermann, 2014), and proxy reconstructions indicate large scale EAIS grounding line retreat in the late Pleistocene (Wilson et al., 2018). While we do not simulate a transition to a marine based EAIS in the Wilkes and Aurora Basins (the pre-MPT EAIS grounding line in this region is already close to its present day configuration), such a process would certainly imprint on ice flow around LDC due to proximity alone. We do find a clear transition of the WAIS configuration around 0.9 Myr in model runs where warm boundary conditions led to a collapse of the WAIS in the late Pliocene but allowed for glaciation during the colder Interglacials in the MPT. We argue, that such a transition between an ice free WAIS and a present day WAIS around 900 ka BP would have a potentially stronger influence on the global climate system (compared to an advance of the EAIS grounded ice margin) via the closing of the gateway between the Ross, Amundsen and Weddell Sea. Additionally, climate conditions pertaining to a retreated configuration of the EAIS ice margin (Raymo et al., 2006) would imply a collapsed WAIS according to ice sheet modelling studies (Golledge et al., 2015; DeConto and Pollard, 2016; Sutter et al., 2016). Our study confirms a strong contribution of the Antarctic Ice Sheet to the LIG sea level highstand, with a mean contribution of 2.5-3 m and a maximum contribution of 4.5 m, which is in line with previous studies by Golledge et al. (2015), Sutter et al. (2016) and DeConto and Pollard (2016). This corroborates the major impact of the Antarctic Ice Sheet on LIG global sea level (Dutton et al., 2015). The spatial pattern of GHF can be decisive in modelling dynamics of the WAIS. Despite this uncertainty, we identify promising candidate sites at Dome Fuji, Dome C and Ridge B which provide favourable conditions for the existence of old ice throughout the last 2 MA. This study illustrates that uncertainties in climate forcing and boundary conditions have a large impact on paleoclimate ice sheet simulations and therefore the assessment of Oldest Ice sites on long time scales. The successful retrieval of an ice core spanning the last 1.5 Myr would provide a transient data benchmark and proxy horizons against which ice sheet models can be tuned and providing insights into a potential major re-arrangement of the East Antarctic coastal margin during the MPT.

Competing interests. O. Eisen is CEIC of The Cryosphere

References

Abe-Ouchi, A., Saito, F., Kawamura, K., Raymo, M. E., Okuno, J., Takahashi, K., and Blatter, H.: Insolation-driven 100,000-year glacial cycles and hysteresis of ice-sheet volume, Nature, 500, 190–+, https://doi.org/10.1038/nature12374, 2013.

Albrecht, T. and Levermann, A.: Fracture-induced softening for large-scale ice dynamics, Cryosphere, 8, 587–605, https://doi.org/Doi

5 10.5194/Tc-8-587-2014, 2014.

An, M. J., Wiens, D. A., Zhao, Y., Feng, M., Nyblade, A., Kanao, M., Li, Y. S., Maggi, A., and Leveque, J. J.: Temperature, lithosphere-asthenosphere boundary, and heat flux beneath the Antarctic Plate inferred from seismic velocities, Journal of Geophysical Research-Solid Earth, 120, 8720–8742, https://doi.org/10.1002/2015jb011917, 2015.

Beckmann, A. and Goosse, H.: A parameterization of ice shelf-ocean interaction for climate models, Ocean Modelling, 5, 157–170,

10 https://doi.org/Pii S1463-5003(02)00019-7 Doi 10.1016/S1463-5003(02)00019-7, 2003.

Bentley, M. J., Cofaigh, C. O., Anderson, J. B., Conway, H., Davies, B., Graham, A. G. C., Hillenbrand, C. D., Hodgson, D. A., Jamieson, S. S. R., Larter, R. D., Mackintosh, A., Smith, J. A., Verleyen, E., Ackert, R. P., Bart, P. J., Berg, S., Brunstein, D., Canals, M., Colhoun, E. A., Crosta, X., Dickens, W. A., Domack, E., Dowdeswell, J. A., Dunbar, R., Ehrmann, W., Evans, J., Favier, V., Fink, D., Fogwill, C. J., Glasser, N. F., Gohl, K., Golledge, N. R., Goodwin, I., Gore, D. B., Greenwood, S. L., Hall, B. L., Hall, K., Hedding, D. W., Hein, A. S.,

15 Hocking, E. P., Jakobsson, M., Johnson, J. S., Jomelli, V., Jones, R. S., Klages, J. P., Kristoffersen, Y., Kuhn, G., Leventer, A., Licht, K., Lilly, K., Lindow, J., Livingstone, S. J., Masse, G., McGlone, M. S., McKay, R. M., Melles, M., Miura, H., Mulvaney, R., Nel, W., Nitsche, F. O., O'Brien, P. E., Post, A. L., Roberts, S. J., Saunders, K. M., Selkirk, P. M., Simms, A. R., Spiegel, C., Stolldorf, T. D., Sugden, D. E., van der Putten, N., van Ommen, T., Verfaillie, D., Vyverman, W., Wagner, B., White, D. A., Witus, A. E., Zwartz, D., and Consortium, R.: A community-based geological reconstruction of Antarctic Ice Sheet deglaciation since the Last Glacial Maximum, Quaternary Science

20 Reviews, 100, 1–9, https://doi.org/10.1016/j.quascirev.2014.06.025, 2014.

Bintanja, R. and van de Wal, R. S. W.: North American ice-sheet dynamics and the onset of 100,000-year glacial cycles, Nature, 454, 869–872, https://doi.org/10.1038/nature07158, <GotoISI>://WOS:000258398600032https://www.nature.com/articles/nature07158.pdf, 2008.

Bueler, E. and Brown, J.: Shallow shelf approximation as a "sliding law" in a thermomechanically coupled ice sheet model, Journal of Geophysical Research-Earth Surface, 114, https://doi.org/Artn F03008 10.1029/2008jf001179, 2009.

25 Cavitte, M. G. P., Parrenin, F., Ritz, C., Young, D. A., Van Liefferinge, B., Blankenship, D. D., Frezzotti, M., and Roberts, J. L.: Accumulation patterns around Dome C, East Antarctica, in the last 73 kyr, Cryosphere, 12, 1401–1414, https://doi.org/10.5194/tc-12-1401-2018, 2018.

Chalk, T. B., Hain, M. P., Foster, G. L., Rohling, E. J., Sexton, P. F., Badger, M. P. S., Cherry, S. G., Hasenfratz, A. P., Haug, G. H., Jaccard, S. L., Martinez-Garcia, A., Palike, H., Pancost, R. D., and Wilson, P. A.: Causes of ice age intensification across the Mid-Pleistocene Transition, Proceedings of the National Academy of Sciences of the United States of America, 114, 13 114–13 119,

30 https://doi.org/10.1073/pnas.1702143114, 2017.

Clark, P. U. and Pollard, D.: Origin of the middle Pleistocene transition by ice sheet erosion of regolith, Paleoceanography, 13, 1–9, https://doi.org/Doi 10.1029/97pa02660, 1998.

de Boer, B., Lourens, L. J., and van de Wal, R. S. W.: Persistent 400,000-year variability of Antarctic ice volume and the carbon cycle is revealed throughout the Plio-Pleistocene, Nature Communications, 5, https://doi.org/ARTN 2999 10.1038/ncomms3999, 2014.

35 DeConto, R. M. and Pollard, D.: Contribution of Antarctica to past and future sea-level rise, Nature, 531, 591–597, https://doi.org/10.1038/nature17145, 2016.

Depoorter, M. A., Bamber, J. L., Griggs, J. A., Lenaerts, J. T. M., Ligtenberg, S. R. M., van den Broeke, M. R., and Moholdt, G.: Calving
    fluxes and basal melt rates of Antarctic ice shelves, Nature, 502, 89–+, 2013.

Dutton, A., Carlson, A. E., Long, A. J., Milne, G. A., Clark, P. U., DeConto, R., Horton, B. P., Rahmstorf, S., and Raymo, M. E.: Sea-level
    rise due to polar ice-sheet mass loss during past warm periods, Science, 349, https://doi.org/ARTN aaa4019 10.1126/science.aaa4019,
5   2015.

Elderfield, H., Ferretti, P., Greaves, M., Crowhurst, S., McCave, I. N., Hodell, D., and Piotrowski, A. M.: Evolution of Ocean Temperature
    and Ice Volume Through the Mid-Pleistocene Climate Transition, Science, 337, 704–709, https://doi.org/10.1126/science.1221294, 2012.

Feldmann, J., Albrecht, T., Khroulev, C., Pattyn, F., and Levermann, A.: Resolution-dependent performance of grounding line motion in
    a shallow model compared with a full-Stokes model according to the MISMIP3d intercomparison, Journal of Glaciology, 60, 353–360,
10 https://doi.org/10.3189/2014JoG13J093, 2014.

Fischer, H., Severinghaus, J., Brook, E., Wolff, E., Albert, M., Alemany, O., Arthern, R., Bentley, C., Blankenship, D., Chappellaz, J., Creyts,
    T., Dahl-Jensen, D., Dinn, M., Frezzotti, M., Fujita, S., Gallee, H., Hindmarsh, R., Hudspeth, D., Jugie, G., Kawamura, K., Lipenkov, V.,
    Miller, H., Mulvaney, R., Parrenin, F., Pattyn, F., Ritz, C., Schwander, J., Steinhage, D., van Ommen, T., and Wilhelms, F.: Where to find
    1.5 million yr old ice for the IPICS "Oldest-Ice" ice core, Climate of the Past, 9, 2489–2505, https://doi.org/Doi 10.5194/Cp-9-2489-2013,
15 2013.

Fretwell, P., Pritchard, H. D., Vaughan, D. G., Bamber, J. L., Barrand, N. E., Bell, R., Bianchi, C., Bingham, R. G., Blankenship, D. D.,
    Casassa, G., Catania, G., Callens, D., Conway, H., Cook, A. J., Corr, H. F. J., Damaske, D., Damm, V., Ferraccioli, F., Forsberg, R., Fujita,
    S., Gim, Y., Gogineni, P., Griggs, J. A., Hindmarsh, R. C. A., Holmlund, P., Holt, J. W., Jacobel, R. W., Jenkins, A., Jokat, W., Jordan,
    T., King, E. C., Kohler, J., Krabill, W., Riger-Kusk, M., Langley, K. A., Leitchenkov, G., Leuschen, C., Luyendyk, B. P., Matsuoka, K.,
20 Mouginot, J., Nitsche, F. O., Nogi, Y., Nost, O. A., Popov, S. V., Rignot, E., Rippin, D. M., Rivera, A., Roberts, J., Ross, N., Siegert,
    M. J., Smith, A. M., Steinhage, D., Studinger, M., Sun, B., Tinto, B. K., Welch, B. C., Wilson, D., Young, D. A., Xiangbin, C., and
    Zirizzotti, A.: Bedmap2: improved ice bed, surface and thickness datasets for Antarctica, Cryosphere, 7, 375–393, https://doi.org/Doi
    10.5194/Tc-7-375-2013, 2013.

Frieler, K., Clark, P. U., He, F., Buizert, C., Reese, R., Ligtenberg, S. R. M., van den Broeke, M. R., Winkelmann, R., and Levermann, A.:
25 Consistent evidence of increasing Antarctic accumulation with warming, Nature Climate Change, 5, 348–352, 2015.

Gladstone, R. M., Payne, A. J., and Cornford, S. L.: Parameterising the grounding line in flow-line ice sheet models, Cryosphere, 4, 605–619,
    https://doi.org/Doi 10.5194/Tc-4-605-2010, 2010.

Golledge, N. R., Menviel, L., Carter, L., Fogwill, C. J., England, M. H., Cortese, G., and Levy, R. H.: Antarctic contribution to meltwater
    pulse 1A from reduced Southern Ocean overturning, Nature Communications, 5, https://doi.org/ARTN 5107 10.1038/ncomms6107, 2014.

30 Golledge, N. R., Kowalewski, D. E., Naish, T. R., Levy, R. H., Fogwill, C. J., and Gasson, E. G. W.: The multi-millennial Antarctic commit-
    ment to future sea-level rise, Nature, 526, 421–+, https://doi.org/10.1038/nature15706, 2015.

Jouzel, J., Masson-Delmotte, V., Cattani, O., Dreyfus, G., Falourd, S., Hoffmann, G., Minster, B., Nouet, J., Barnola, J. M., Chappellaz,
    J., Fischer, H., Gallet, J. C., Johnsen, S., Leuenberger, M., Loulergue, L., Luethi, D., Oerter, H., Parrenin, F., Raisbeck, G., Raynaud,
    D., Schilt, A., Schwander, J., Selmo, E., Souchez, R., Spahni, R., Stauffer, B., Steffensen, J. P., Stenni, B., Stocker, T. F., Tison, J. L.,
35 Werner, M., and Wolff, E. W.: Orbital and millennial Antarctic climate variability over the past 800,000 years, Science, 317, 793–796,
    https://doi.org/Doi 10.1126/Science.1141038, 2007.

Karlsson, N. B., Binder, T., Eagles, G., Helm, V., Pattyn, F., Van Liefferinge, B., and Eisen, O.: Glaciological characteristics in the Dome
    Fuji region and new assessment for "Oldest Ice", Cryosphere, 12, 2413–2424, https://doi.org/10.5194/tc-12-2413-2018, 2018.

Konrad, H., Thoma, M., Sasgen, I., Klemann, V., Grosfeld, K., Barbi, D., and Martinec, Z.: The Deformational Response of a Viscoelastic Solid Earth Model Coupled to a Thermomechanical Ice Sheet Model, Surveys in Geophysics, 35, 1441–1458, https://doi.org/Doi 10.1007/S10712-013-9257-8, 2014.

Larour, E., Morlighem, M., Seroussi, H., Schiermeier, J., and Rignot, E.: Ice flow sensitivity to geothermal heat flux of Pine Island Glacier, 5 Antarctica, Journal of Geophysical Research-Earth Surface, 117, https://doi.org/Artn F04023 10.1029/2012jf002371, 2012.

Lazeroms, W. M. J., Jenkins, A., Gudmundsson, G. H., and van de Wal, R. S. W.: Modelling present-day basal melt rates for Antarctic ice shelves using a parametrization of buoyant meltwater plumes, Cryosphere, 12, 49–70, https://doi.org/10.5194/tc-12-49-2018, 2018.

Lisiecki, L. E. and Raymo, M. E.: A Pliocene-Pleistocene stack of 57 globally distributed benthic delta O-18 records, Paleoceanography, 20, https://doi.org/Artn Pa1003 10.1029/2004pa001071, 2005.

10 Locarnini, R. A., Mishonov, A. V., Antonov, J. I., Boyer, T. P., Garcia, H. E., Baranova, O. K., Zweng, M. M., and Johnson, D. R.: World Ocean Atlas 2009, Volume 1: Temperature., NOAA Atlas NESDIS 68, U.S. Government Printing Office, 2010.

Lunt, D. J., Abe-Ouchi, A., Bakker, P., Berger, A., Braconnot, P., Charbit, S., Fischer, N., Herold, N., Jungclaus, J. H., Khon, V. C., Krebs-Kanzow, U., Langebroek, P. M., Lohmann, G., Nisancioglu, K. H., Otto-Bliesner, B. L., Park, W., Pfeiffer, M., Phipps, S. J., Prange, M., Rachmayani, R., Renssen, H., Rosenbloom, N., Schneider, B., Stone, E. J., Takahashi, K., Wei, W., Yin, Q., and Zhang, Z. S.: A 15 multi-model assessment of last interglacial temperatures, Climate of the Past, 9, 699–717, 2013.

Lythe, M. B., Vaughan, D. G., and Consortium, B.: BEDMAP: A new ice thickness and subglacial topographic model of Antarctica, Journal of Geophysical Research-Solid Earth, 106, 11 335–11 351, https://doi.org/Doi 10.1029/2000jb900449, 2001.

Martos, Y. M., Catalan, M., Jordan, T. A., Golynsky, A., Golynsky, D., Eagles, G., and Vaughan, D. G.: Heat Flux Distribution of Antarctica Unveiled, Geophysical Research Letters, 44, 11 417–11 426, https://doi.org/10.1002/2017gl075609, 2017.

20 Mengel, M. and Levermann, A.: Ice plug prevents irreversible discharge from East Antarctica, Nature Climate Change, 4, 451–455, https://doi.org/Doi 10.1038/Nclimate2226, 2014.

Michel, A., Schwander, J., and Fischer, H.: Transient Modeling of Borehole Temperature and Basal Melting in an Ice Sheet, Master Thesis, Climate and Environmental Physics Institute, University of Bern, 2016.

Parrenin, F., Cavitte, M. G. P., Blankenship, D. D., Chappellaz, J., Fischer, H., Gagliardini, O., Masson-Delmotte, V., Passalacqua, O., Ritz, 25 C., Roberts, J., Siegert, M. J., and Young, D. A.: Is there 1.5-million-year-old ice near Dome C, Antarctica?, Cryosphere, 11, 2427–2437, https://doi.org/10.5194/tc-11-2427-2017, 2017.

Passalacqua, O., Ritz, C., Parrenin, F., Urbini, S., and Frezzotti, M.: Geothermal flux and basal melt rate in the Dome C region inferred from radar reflectivity and heat modelling, Cryosphere, 11, 2231–2246, https://doi.org/10.5194/tc-11-2231-2017, 2017.

Pfeiffer, M. and Lohmann, G.: Greenland Ice Sheet influence on Last Interglacial climate: global sensitivity studies performed with an 30 atmosphere-ocean general circulation model, Climate of the Past, 12, 1313–1338, https://doi.org/10.5194/cp-12-1313-2016, 2016.

Pollard, D. and DeConto, R. M.: Modelling West Antarctic ice sheet growth and collapse through the past five million years, Nature, 458, 329–333, 2009.

Pollard, D. and DeConto, R. M.: Description of a hybrid ice sheet-shelf model, and application to Antarctica, Geoscientific Model Development, 5, 1273–1295, https://doi.org/10.5194/gmd-5-1273-2012, 2012.

35 Purucker, M. E.: Geothermal heat flux data set based on low res- olution observations collected by the CHAMP satellite be- tween 2000 and 2010, and produced from the MF-6 model following the technique described in Fox Maule et al. (2005), retrieved from: https:core2.gsfc.nasa.govresearchpuruckerheatflux_updates.html, 2013.

Raymo, M. E. and Huybers, P.: Unlocking the mysteries of the ice ages, Nature, 451, 284–285, https://doi.org/10.1038/nature06589, 2008.

Raymo, M. E., Lisiecki, L. E., and Nisancioglu, K. H.: Plio-pleistocene ice volume, Antarctic climate, and the global delta O-18 record, Science, 313, 492–495, https://doi.org/10.1126/science.1123296, 2006.

Reese, R., Gudmundsson, G. H., Levermann, A., and Winkelmann, R.: The far reach of ice-shelf thinning in Antarctica, Nature Climate Change, 8, 53–+, https://doi.org/10.1038/s41558-017-0020-x, 2018.

5 Rignot, E., Jacobs, S., Mouginot, J., and Scheuchl, B.: Ice-Shelf Melting Around Antarctica, Science, 341, 266–270, https://doi.org/10.1126/science.1235798, 2013.

Rohling, E. J., Foster, G. L., Grant, K. M., Marino, G., Roberts, A. P., Tamisiea, M. E., and Williams, F.: Sea-level and deep-sea-temperature variability over the past 5.3 million years (vol 508, pg 477, 2014), Nature, 510, 432–432, https://doi.org/10.1038/nature13488, 2014.

Schoof, C.: Coulomb Friction and Other Sliding Laws in a Higher-Order Glacier Flow Model, Mathematical Models & Methods in Applied
10   Sciences, 20, 157–189, https://doi.org/10.1142/S0218202510004180, 2010.

Shapiro, N. M. and Ritzwoller, M. H.: Inferring surface heat flux distributions guided by a global seismic model: particular application to Antarctica, Earth and Planetary Science Letters, 223, 213–224, https://doi.org/Doi 10.1016/J.Epsl.2004.04.011, 2004.

Snyder, C. W.: Evolution of global temperature over the past two million years, Nature, 538, 226–+, https://doi.org/10.1038/nature19798, 2016.

15 Stepanek, C. and Lohmann, G.: Modelling mid-Pliocene climate with COSMOS, Geoscientific Model Development, 5, 1221–1243, https://doi.org/10.5194/gmd-5-1221-2012, 2012.

Sutter, J., Gierz, P., Grosfeld, K., Thoma, M., and Lohmann, G.: Ocean temperature thresholds for Last Interglacial West Antarctic Ice Sheet collapse, Geophysical Research Letters, 43, 2675–2682, https://doi.org/10.1002/2016gl067818, 2016.

Tigchelaar, M., Timmermann, A., Pollard, D., Friedrich, T., and Heinemann, M.: Local insolation changes enhance Antarctic interglacials:
20   Insights from an 800,000-year ice sheet simulation with transient climate forcing, Earth and Planetary Science Letters, 495, 69–78, https://doi.org/10.1016/j.epsl.2018.05.004, 2018.

Van Liefferinge, B. and Pattyn, F.: Using ice-flow models to evaluate potential sites of million year-old ice in Antarctica, Climate of the Past, 9, 2335–2345, https://doi.org/Doi 10.5194/Cp-9-2335-2013, 2013.

Van Liefferinge, B., Pattyn, F., Cavitte, M. G. P., Karlsson, N. B., Young, D. A., Sutter, J., and Eisen, O.: Promising Oldest Ice sites in East
25   Antarctica based on thermodynamical modelling, Cryosphere, 12, 2773–2787, https://doi.org/10.5194/tc-12-2773-2018, 2018.

van Wessem, J. M., Reijmer, C. H., Morlighem, M., Mouginot, J., Rignot, E., Medley, B., Joughin, I., Wouters, B., Depoorter, M. A., Bamber, J. L., Lenaerts, J. T. M., van de Berg, W. J., van den Broeke, M. R., and van Meijgaard, E.: Improved representation of East Antarctic surface mass balance in a regional atmospheric climate model, Journal of Glaciology, 60, 761–770, https://doi.org/10.3189/2014JoG14J051, 2014.

30 Werner, M., Jouzel, J., Masson-Delmotte, V., and Lohmann, G.: Reconciling glacial Antarctic water stable isotopes with ice sheet topography and the isotopic paleothermometer, Nature Communications, 9, https://doi.org/ARTN 3537 10.1038/s41467-018-05430-y, 2018.

Wilson, D. J., Bertram, R. A., Needham, E. F., van de Flierdt, T., Welsh, K. J., McKay, R. M., Mazumder, A., Riesselman, C. R., Jimenez-Espejo, F. J., and Escutia, C.: Ice loss from the East Antarctic Ice Sheet during late Pleistocene interglacials, Nature, 561, 383–+, https://doi.org/10.1038/s41586-018-0501-8, 2018.

35 Winkelmann, R., Martin, M. A., Haseloff, M., Albrecht, T., Bueler, E., Khroulev, C., and Levermann, A.: The Potsdam Parallel Ice Sheet Model (PISM-PIK) - Part 1: Model description, Cryosphere, 5, 715–726, https://doi.org/Doi 10.5194/Tc-5-715-2011, 2011.

Young, D. A., Roberts, J. L., Ritz, C., Frezzotti, M., Quartini, E., Cavitte, M. G. P., Tozer, C. R., Steinhage, D., Urbini, S., Corr, H. F. J., van Ommen, T., and Blankenship, D. D.: High-resolution boundary conditions of an old ice target near Dome C, Antarctica, Cryosphere, 11, 1897–1911, https://doi.org/10.5194/tc-11-1897-2017, 2017.

Yu, H., Rignot, E., Seroussi, H., and Morlighem, M.: Retreat of Thwaites Glacier, West Antarctica, over the next 100 years using various ice
5   flow models, ice shelf melt scenarios and basal friction laws, The Cryosphere Discussions, 2018, 1–19, https://doi.org/10.5194/tc-2018-104, 2018.
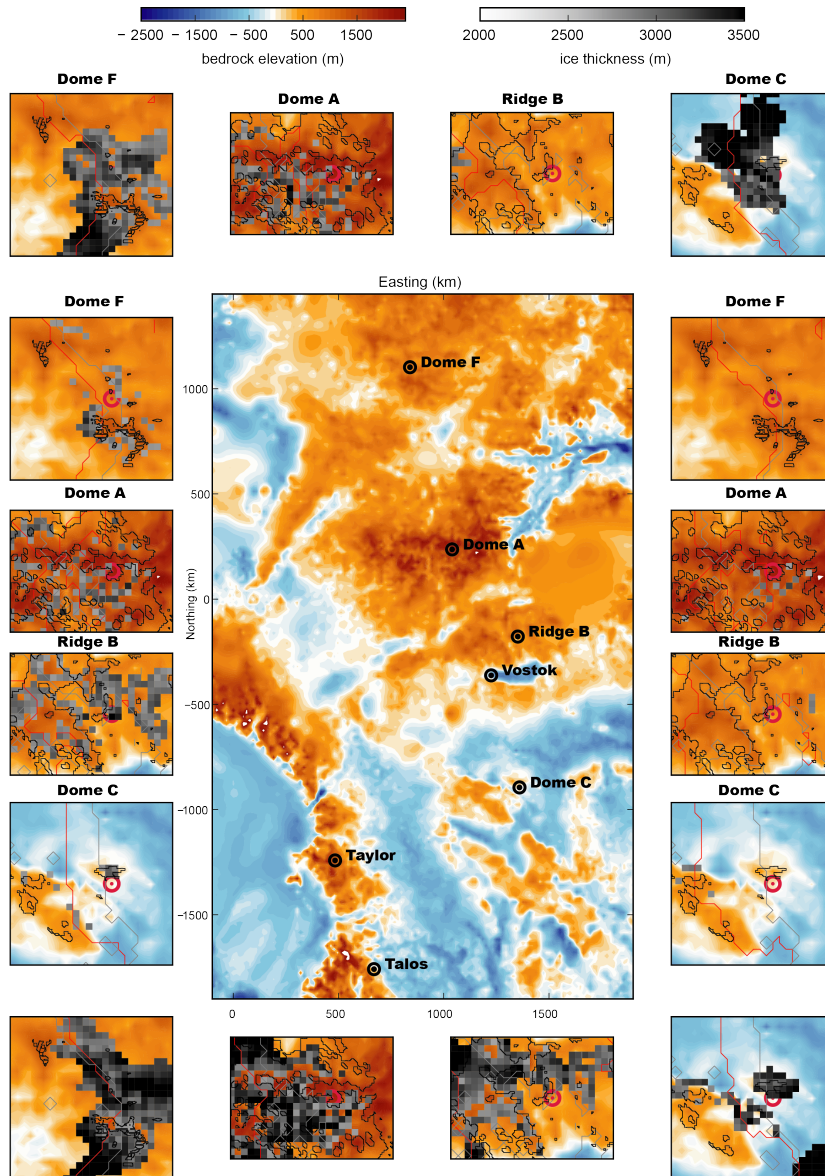
Figure 9. "Triptych" with comparison between regions of Oldest Ice identified in this study and in Van Liefferinge and Pattyn (2013) (Ridge B, Dome A) and Van Liefferinge et al. (2018) (Dome C, Dome Fuji) outlined in black. Regions of oldest ice are defined as grid nodes where ice thickness is larger than 2000 m, basal melting is zero and surface ice velocity slower than 1 m/a. The left and right columns show magnified sections centred at Dome Fuji, Ridge B and Dome C for identical parameter sets and forcing but different geothermal heat flux (left from Shapiro and Ritzwoller (2004), right from Martos et al. (2017), the bottom row shows Purucker (2013) GHF forcing). The top row shows the same run but with GHF from An et al. (2015). The red dashed line in blown up regions depicts simulated present day ice divide (defined as position where surface gradient switches sign), while the dashed grey line depicts the present day ice divide as computed from BEDMAP2.